DOI: 10.1002/chem.200700031

Cell-Specific and Nuclear Targeting with $[M(CO)_3]^+$ (M = ^{99m}Tc, Re)-Based Complexes

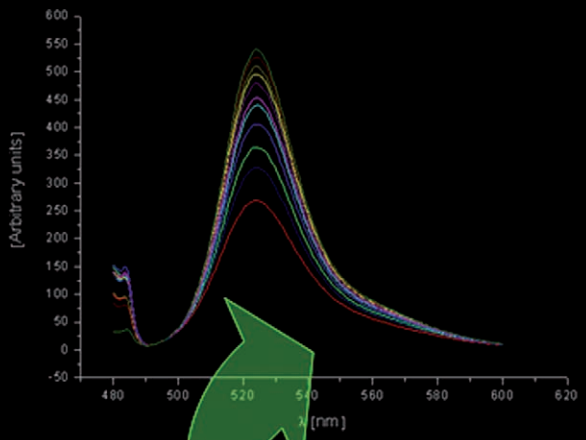

DAPI

DNA

Acridine Orange

Cell-Specific and Nuclear Targeting with $[M(CO)_3]^+$ (M = ^{99m}Tc, Re)-Based Complexes Conjugated to Acridine Orange and Bombesin

Nikos Agorastos,[a] Lubor Borsig,[b] Anabelle Renard,[c] Philipp Antoni,[a] Giampietro Viola,[d] Bernhard Spingler,[a] Philipp Kurz,[a] and Roger Alberto*[a]

Abstract: Receptor-specific nuclear targeting requires trifunctional metal complexes. We have synthesized [M-(L^2-pept)(L^1-acr)$(CO)_3$] (pept = peptide; acr = acridine-based agent) in which the *fac*-$[M(CO)_3]^+$ moiety (1st function, M = ^{99m}Tc, Re) couples an acridine-based nuclear-targeting agent (2nd function, L^1-acr) and the specific cell-receptor-binding peptide bombesin (3rd function, L^2-pept). The metal-mediated coupling is based on the mixed ligand [2+1] principle. The nuclear targeting agents have been derivatised with an isocyanide group for monodentate (L^1) and bombesin (BBN) with a bidentate ligand (L^2) for complexation to *fac*-$[M(CO)_3]^+$. For nuclear uptake studies, the model complexes $[Re(L^2)(L^1\text{-acr})(CO)_3]$ (L^2 = pyridine-2-carboxylic acid and pyridine-2,4-dicarboxylic acid) were synthesized and structurally characterized. We selected acridine derivatives as nuclear-targeting agents, because they are very good nucleus-staining agents and exhibit strong fluorescence. Despite the bulky metal complexes attached to acridine, all $[Re(L^2)(L^1\text{-acr})(CO)_3]$ showed high accumulation in the nuclei of PC3 and B16F1 cells, as evidenced by fluorescence microscopy. For radiopharmaceutical purposes, the ^{99m}Tc analogues have been prepared and radioactivity distribution confirmed the fluorescence results. Coupling of BBN to L^2 gave the receptor-selective complexes $[M(L^2\text{-BBN})(L^1\text{-acr})(CO)_3]$. Whereas no internalization was found with B16F1 cells, fluorescence microscopy on PC3 cells bearing the BBN receptor showed high and rapid uptake by receptor-mediated endocytosis into the cytoplasm, but not into the nucleus.

Keywords: bioorganometallics · fluorescence · nuclear targeting · rhenium · technetium

Introduction

Current radiopharmaceutical research focuses on cell-specific receptor-targeting agents for the diagnosis or therapy of cancer and other diseases.[1–3] After receptor binding, subsequent internalisation and accumulation of the radioconjugates, the radionuclides should not be washed out, thereby ensuring both therapeutic effect and imaging. Therapeutic effects from β-emitting radionuclides, such as ^{131}I, ^{176}Lu or $^{186/188}$Re, to name only a few, are achieved inside and amongst the cells by the cross-firing effect of high-energy β^- particles. Essential molecules, such as DNA or intracellular proteins, are affected by direct hits or by reactive oxygen species (ROS) generated, for example, through ionisation of water or oxygen.[4–6] Cell death might occur by apoptosis or by necrosis. Whereas radioimaging allows for sensitive, non-invasive in vivo imaging of receptor distribution and biological processes at reasonable spatial resolution, it is barely able to visualize the behaviour of compounds on the cellular or subcellular level. It would be desirable to follow in vitro in real time the pathway of a radiolabelled compound in

[a] N. Agorastos, P. Antoni, Dr. B. Spingler, Dr. P. Kurz, Prof. Dr. R. Alberto
Institute of Inorganic Chemistry
University of Zürich
Winterthurerstrasse 190, 8057 Zurich (Switzerland)
Fax: (+41) 44-635-68-03
E-mail: ariel@aci.unizh.ch

[b] Dr. L. Borsig
Institute of Physiology
University of Zürich
Winterthurerstrasse 190, 8057 Zurich (Switzerland)

[c] Dr. A. Renard
Institute of Organic Chemistry
University of Zürich
Winterthurerstrasse 190, 8057 Zurich (Switzerland)

[d] Dr. G. Viola
Department of Pharmaceutical Sciences
University of Padova
via Marzolo 5, 35131 Padova (Italy)

order to know its ultimate site of accumulation. Fluorescence microscopy is a highly suited and powerful tool for this purpose. Hence, structurally identical fluorescent and radioactive probes would allow the elucidation of the microscopic track of the compound inside the cell, while imaging with scintigraphy from outside.[7]

Receptor targeting is the common strategy in radiopharmacy, but cell-specific targeting of the nucleus is less developed and essentially a "no-go" area (in radiopharmacy). Beside purely organic compounds, various metal complexes have recently been shown to stain cellular nucleus compartments very precisely, at low concentration and with high resolution.[8,9] Nuclear targeting is challenging, because cell-specific targeting and penetration of the nucleus wall have to be combined. Some amino acid sequences, such as chemotactic TAT or nuclear localising sequence (NLS) peptides, have been reported[7,10,11] and are known as carriers into the nucleus, but their combination with cell-receptor-specific agents has not been described to our knowledge. Nuclear-targeting agents in combination with cell-receptor-specific ligands would provide a new strategy for radionuclide therapy: short-range, high-LET Auger electron emitters (LET = linear energy transfer) such as ^{125}I, ^{111}In or ^{99m}Tc as well as alpha emitters could be delivered to the nucleus to exert their therapeutic action directly to DNA or RNA. The dose deposited very locally is much higher than in the case of low-LET β-emitters.[12–14]

To assess the possibility of cell-specific nuclear targeting with metal complexes, we have combined the neuropeptide bombesin (BBN) and acridine derivatives.[15] Bombesin is neuropeptide of 14 amino acids, originally isolated from frog skin, with high affinity for the gastrin-releasing peptide (GRP) receptor. Acridine-based organic compounds are highly fluorescent and may act as carriers for pendent molecules into the cell nucleus. The two biological functions are linked to each other by the $[M(CO)_3]^+$ moiety, following the so-called mixed ligand [2+1] approach.[16] The central complex fragment as the radioactive probe represents the third function. The concept of these trifunctional metal complexes for cell-specific nuclear targeting is depicted in Scheme 1.

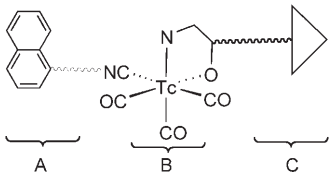

Scheme 1. Schematized representation of a trifunctional radiopharmaceutical: A) nuclear-targeting molecule, B) radioactive metal complex for imaging or therapy, C) specific cell-receptor-targeting molecule.

Results and Discussion

Synthetic procedures: We have recently reported about trifunctional metal complexes composed of the fluorescent organic dye pyrene, a nuclear localising sequence (NLS) peptide and a tridentate chelator coordinated to the $[^{99m}Tc(CO)_3]^+$ moiety.[17] Although the proof of concept for nuclear uptake was given, the syntheses of those conjugates were lengthy and of little flexibility for drug development with respect to intercalator- and receptor-targeting vector variation. Furthermore, it did not easily allow the introduction of a further cell-specific targeting agent such as a peptide. Acridine derivatives are standard compounds for nuclear staining, because they are strongly fluorescent and reasonably water soluble.[18] They can be derivatised at several positions, while still keeping their ability to reach the cell nucleus intact. To facilitate the combination of cell-specific and nuclear-targeting agents, we employed the mixed ligand [2+1] approach. One of the active molecules is bound to the metal through a bidentate and the other one through a monodentate ligand. The isocyanide group is a strong monodentate ligand and suitable for introduction in the basic acridine leads. Synthetically, we performed the reaction of ethylene diamine with acridine carboxylic acid **1** to yield compound **2**. Formamidation of the terminal amino group in **2** gave compound **3** and subsequent dehydration gave the isocyanide derivative **4**. To attach a isocyanide moiety to the N10 of acridine orange (**5**), an alkylation with *N*-(4-bromobutyl)formamide was carried out to yield **6** followed again by dehydration to yield the isocyanide derivative **7**. Both synthetic pathways are shown in Scheme 2.

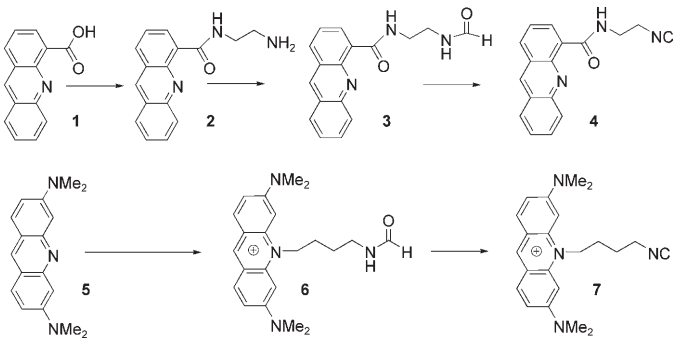

Scheme 2. Synthesis of the monodentate ligands **4** and **7**.

The strategy of conjugating a monodentate isocyanide ligand can be applied to other nuclear-targeting agents as well.[19] Thus, if the receptor-targeting molecule (a peptide for instance) is kept unchanged, the nucleus-targeting function can be altered without substantially varying the overall composition of the trifunctional conjugate. The isocyanide ligands **4** and **7** retained their nucleus-staining properties as could be seen in fluorescence microscopy studies with PC3 and B16F1 cells. Whereas **4** and **7** are not significantly different from their lead compounds, the coupling of a metal complex will significantly increase the overall size and physicochemical properties. Thus, it is crucial to evaluate if complexes based on the $[Re(CO)_3]^+$ core and bound to **4** and **7** would still be nuclear-targeting agents. The remaining two coordination sites (in which the receptor-targeting function will be bound later) must be blocked by a bidentate ligand.

We selected 2,4-pyridinedicarboxylic acid (2,4-pydic) for this purpose. The pyridine nitrogen atom and one of the carboxylato groups coordinate to the metal centre, while the second carboxylate can be used for covalent binding to a peptide. In a first step, reaction of 2,4-pydic with $[Re(OH_2)_3(CO)_3]^{2-}$ in water gave the complex $[Re(OH_2)(2,4\text{-pydic})(CO)_3]$ (**8**) in quantitative yield. In a second step ligands **4** or **7** were reacted with **8** to yield the final model complexes $[Re(\mathbf{4})(2,4\text{-pydic})(CO)_3]$ (**9**) and $[Re(\mathbf{7})(2,4\text{-pydic})(CO)_3]$ (**10**) in good yields (Scheme 3).

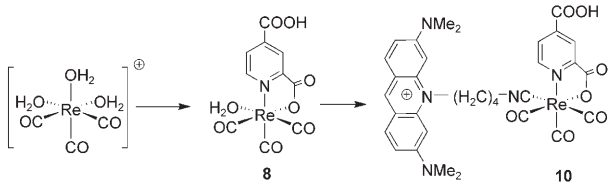

Scheme 3. Synthesis of compound **10** from $[Re(OH_2)_3(CO)_3]^+$ (**7**).

The X-ray structures of complexes **9** and **10** could be elucidated. ORTEP presentations are given in Figures 1 and 2 and important crystallographic data in Table 1.

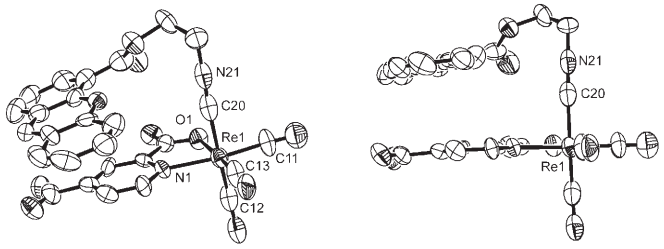

Figure 1. Molecular structure of complex **9**. Solvent and hydrogen atoms are omitted for clarity. Selected bond lengths [Å] and angles [°] for **9** are: Re1–C11 1.901(19), Re1–N1 2.162(12), Re1–O1 2.117(10); C11-Re1-O1 95.5(7), C11-Re1-N1 171.4(8), O1-Re1-N1 76.2(5).

The X-ray crystal structure analysis of **9** shows strong intramolecular interactions between the two aromatic systems acridine and pyridine. The relative orientation of these aromatic π systems reveals that they are almost parallel to each other with a minimal interplanar separation of about 3.43 Å. The intramolecular π stacking of the aromatic rings is strong and defines the molecular structure, rather than the overall molecular properties being important for intermolecular π–π interactions.[20] Presumably, this intramolecular π stacking contributes to the steric hindrance of the complete complex, thereby preventing the acridine moiety from intercalating into the DNA base pairs (see below). In addition complex **9** is negatively charged under physiological conditions, which further disfavours interaction with the DNA due to the DNA's negatively charged phosphate backbone. However, π-stacking interactions could not be confirmed in solution by NOESY NMR experiments.

In contrast to **9**, the crystal structure of complex **10** (Figure 2) shows the acridine orange moiety rotated away from the rest of the complex. Although the solid-state structure does not necessarily mirror the behaviour of **10** in solution, the absence of intramolecular π stacking implies that the compound should be a stronger intercalator (or DNA binder) than **9**, an assumption that could be confirmed by linear dichroism (LD) measurements as described below. The acridinium orange unit in **10** forms a layer of π-stacked aromatic rings together with symmetry-generated molecules. The following hydrogen bridges could be identified: O5···O10 2.84 Å (O5 from a bound carboxylate, oxygen coordinating to Re and O10 (x,y,z) is from a water molecule);

Table 1. Crystallographic data for complexes **9** and **10**.

	9	**10**
formula	$C_{29}H_{23}N_4O_9Re$	$C_{32}H_{34}N_5O_{11}Re$
M_r	757.71	850.84
T [K]	183(2)	183(2)
λ [Å]	0.71073	0.71073
crystal system	triclinic	triclinic
space group	$P\bar{1}$	$P\bar{1}$
a [Å]	8.0021(11)	7.7329(13)
b [Å]	13.6225(15)	15.175(3)
c [Å]	13.7436(19)	16.851(3)
α [°]	82.058(15)	71.09(2)
β [°]	76.173(16)	84.845(19)
γ [°]	85.371(15)	77.94(5)
V [Å^3]	1439.03(3)	1828.9(5)
Z	2	2
ρ_{calcd} [Mg m^{-3}]	1.749	1.545
μ [mm^{-1}]	4.283	3.384
max 2θ [°]	24.0	25.95
unique reflns	4297	6667
G.o.fit on F^2	0.801	0.738
$R^{[a,b]}$	0.0655	0.0778
$wR2^{[a,c]}$	0.1381	0.1769

[a] Observation criterion: $[I>2\sigma(I)]$. [b] $R=\Sigma||F_o|-|F_c||/\Sigma|F_o|$. [c] $wR2=\{\Sigma[w(F_o^2-F_c^2)^2]/\Sigma[w(F_o^2)^2]\}^{1/2}$.

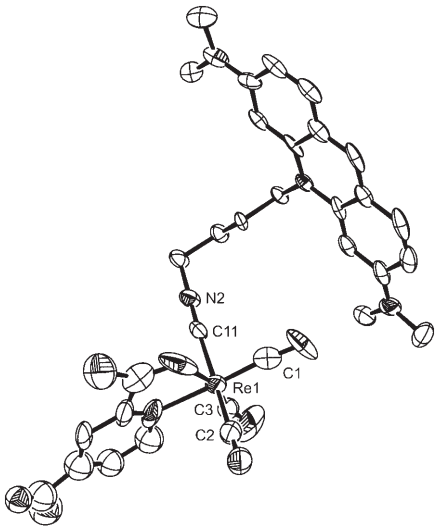

Figure 2. Molecular structure of complex **10**. Solvent molecules and hydrogen atoms are omitted for clarity. Selected bond lengths [Å] and angles [°]for **10** are: Re1–C11 2.080(15), Re1–N1 2.264(19), Re1–O5 1.88(3), Re1–C3 1.494(16), Re1–C1 1.885(15), Re1–C2 1.915(15); C111-Re1-O5 85.0(6), C11-Re1-N1 90.5(5), O5-Re1-N1 73.9(8).

O6···O11 2.81 Å (O6 is a free carboxylate oxygen atom and O11 $(x,y-1,z)$ is from a water molecule); O7···O12 2.72 Å (O7 is a free carboxylate oxygen atom and O12 $(-x-1,-y+1,-z)$ is from a water molecule); O7···O13 2.66 Å (O7 is a free carboxylate oxygen atom and O13 $(x+1,y-1,z)$ is from a water molecule).

The bidentate ligand 2,4-pydic can be coupled to the receptor-targeting peptide bombesin (BBN) by standard peptide synthetic methods directly on a solid-phase support. BBN binds to the GRP receptor, which is over-expressed on many tumour cell lines and therefore relevant for cancer imaging and therapy. The peptide has been extensively studied for labelling with ^{111}In or ^{99m}Tc.[21] Bombesin was synthesised by using standard solid-phase technology. In the last step prior to full deprotection and cleavage from the solid phase, the 2-monomethyl ester of 2,4-pydic was coupled to the BBN N terminus by using BOP activation (BOP = (benzotriazol-1-yloxy)tris(dimethylamino)phosphonium hexafluorophosphate). Deprotection and cleavage from the solid phase, followed by HPLC purification gave the final product BBN–(2,4-pydic) (**11**) in good yield.

ESI-MS analysis confirmed the authenticity of the product m/z 961.51 $[M]^+$. In a next step, **11** was reacted with $[Re(OH_2)_3(CO)_3]^+$ in water to get **12** in 92% yield. ESI-MS gave the correct mass of m/z 1230.93 $[M-OH_2]^+$. The final step to compound **13** consisted in the introduction of the nuclear targeting moiety **7**. Reaction of **12** with **7** in water gave compound **13** (Scheme 4). ESI-MS showed the correct mass

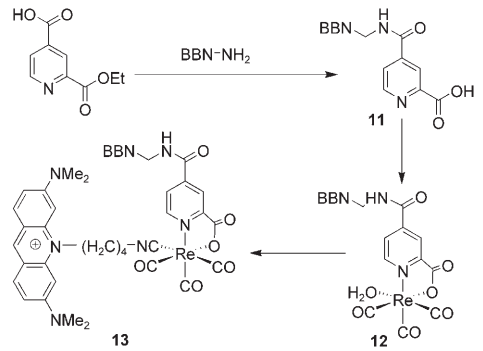

Scheme 4. Derivatisation of bombesin with 2,4-pydic, complexation with $[Re(OH_2)_3(CO)_3]^+$ and introduction of the nuclear-targeting agent to yield the trifunctional compound **13**.

of 1578.76 and infrared spectroscopy evidenced the vibration frequencies of the carbonyl ligands ν(CO) at 1904 and 2023 cm^{-1}, respectively. Compound **13** represents a first example of a model trifunctional complex that can also be prepared with ^{99m}Tc by an analogous pathway. In complex **13**, the nuclear-targeting molecule **7**, bound through the isocyanide to the rhenium centre, the receptor-targeting biomolecule BBN and the metal centre are combined into a single molecular entity.

Binding constants and binding mode: Acridine-based organic dyes are known to be strong DNA binders. Acridine orange has an affinity constant of 1.18×10^5 M^{-1} and the parent compound acridine one of 4.50×10^5 M^{-1}.[22] Both molecules show high and fast accumulation in the cell nucleus. Their real-time uptake has been studied by fluorescence microscopy.[23,24] As a base for nuclear uptake studies, it is of key importance to know whether **9** and **10** are still penetrating the cell wall to reach the nucleus. Considering the fact that bulky metal complexes are attached to these nuclear-targeting agents, one might expect that this ability is might be hampered or lost. It is also essential to determine the affinity and binding mode of complexes **9** and **10** to DNA in order to assess a tight interaction that is required for imaging or therapy. We determined the affinity constants by fluorescence titration of the ligands **4** and **7** by calf thymus DNA (ct DNA) and with complexes **9** and **10**, respectively. We did not find any fluorescence enhancement or absorption maximum shift with **4** or **9**, indicating that these compounds are not binding in an intercalative way. On the other hand, ligand **7** and complex **10** showed a strong fluorescence increase and red shifts of the emission maxima upon addition of ct DNA, indicating intercalation as has been observed earlier for a Pt^{II} complex bound to acridine orange.[18]

Figure 3 shows the dependence of the relative emission intensities of the complex **10** as a function of the concentra-

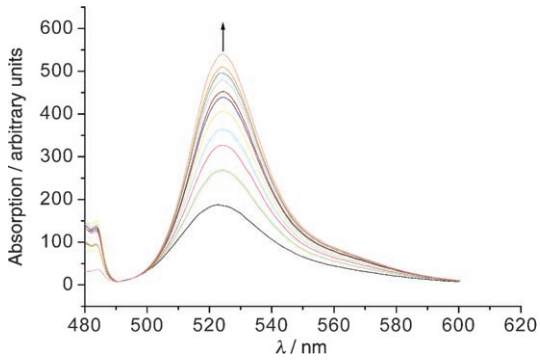

Figure 3. Fluorescence enhancement upon addition of ct DNA in buffer to a solution of complex **10**.

tion of DNA in a phosphate-buffered solution at pH 7.4. The concentration of **10** was kept constant. Upon addition of ct DNA, the emission intensity increased steadily and was enhanced about threefold at a saturation [DNA]/[Re] ratio of 20:1. The increase in luminescence intensities of **10**, together with the hypochromic shift observed in the electronic absorption spectra ($\Delta\lambda = 4$ nm), are clear indicators for the intercalation of the acridine moiety of rhenium complex **10** into the DNA double helix.[25,26] Isothermal titration calorimetry (ITC) measurements allows the very sensitive determination of affinity constants K_i by titration of **7** and **10** into an aqueous solution of ct DNA. The heat flow measured by ITC is in direct correlation with the free energy ($\Delta G_{overall}$) released by the intercalation of **7** and **10**, respectively. The first affinity constant obtained for ligand **7** was $K_i = 2.13\times$

$10^5 \pm 0.43 \times 10^5\,\text{M}^{-1}$ ($\Delta H_1 = -13.0 \pm 0.4\,\text{kcal mol}^{-1}$), which is more accurate than the values obtained from fluorescence spectra. For the rhenium complex **10**, $K_i = 1.13 \times 10^5 \pm 0.07 \times 10^5\,\text{M}^{-1}$ ($\Delta H_1 = -8.9 \pm 0.2\,\text{kcal mol}^{-1}$) is smaller than for ligand **7** as expected. Nevertheless, the values indicate a high affinity of **10** for ct DNA although the bulky metal residue attached to the targeting agent affects the intercalation by about a factor of two.

The determination of K_i is not sufficient on its own to identify a particular mode of interaction. Linear dichroism (LD) measurements are more conclusive, because this methodology has been shown to be an efficient tool to evaluate the distinct binding mode between a dye and nucleic acids.[27] Thus, we recorded the absorption and LD spectra in the presence of ct DNA. The corresponding spectra are depicted in Figure 4 for the ligand **4** and complex **9**.

Figure 4 (top) confirms the intercalation of acridine derivative **4** in ct DNA. It could be expected that complex **9** behaves similarly, but fluorescence titrations implied already that this is not the case. LD spectra confirm this assumption. Even at a very high dye/DNA ratio no linear dichroism signals were induced in the absorption region of **9**, confirming the fluorescence titration experiments. Although no evidence from NOESY NMR experiments could be obtained, the intramolecular π--π stacking as observed in the X-ray structure is likely to compete for DNA binding.

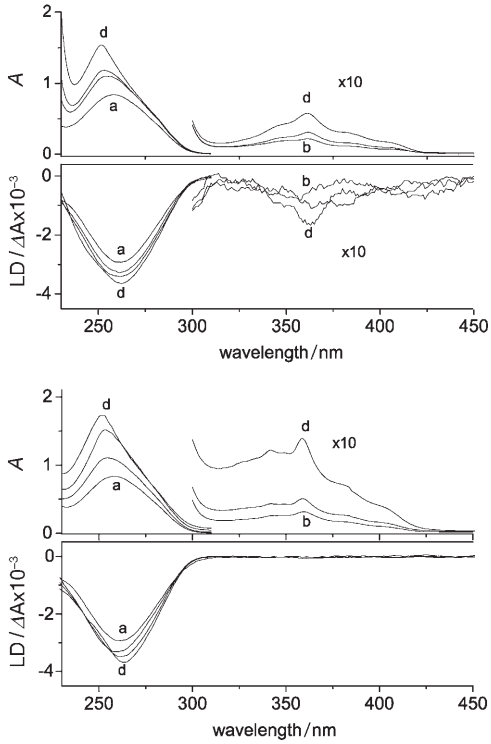

Figure 4. Absorption and LD spectra of ligand **4** (top) and complex **9** (bottom). Spectra were recorded in phosphate buffer 10 mM, pH 7.2, at different [DNA-bp]/[dye] ratios. a) no dye; b) 25; c) 12; d) 5.

The situation is different for **7** and **10**. The LD signals of **7** were negative at all dye/DNA mixing ratios, both in the UV region at which the DNA and the dye absorb, as well as for wavelengths at which only the dye absorbs (Figure 5, top). The LD signals in the long-wavelength absorption regions of the dye (400–600 nm) were negative in the presence of DNA, indicating an induced orientation of the ligand chromophore upon binding to ct DNA. A significant increase of the LD signal intensities in the absorption band of the DNA bases (260 nm) was also observed, suggesting that the ability of the DNA molecules to orient along the flow lines is increased upon binding to this compound.

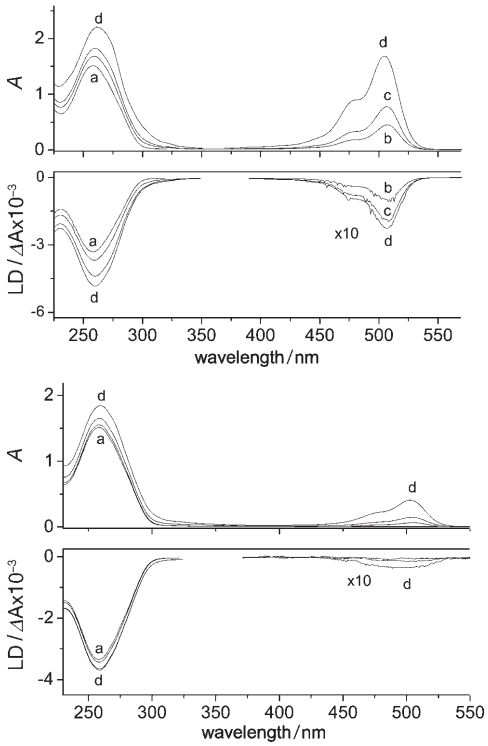

Figure 5. Absorption and LD spectra of ligand **7** (top) and complex **10** (bottom). Spectra were recorded in phosphate buffer 10 mM, pH 7.2, at different [DNA-bp]/[dye] ratios a) no dye; b) 25; c) 12; d) 5.

A similar result is obtained for compound **10**. A small but significant LD signal can be observed in the dye absorption region (Figure 5, bottom), although only at the highest dye/[DNA] ratio employed. This suggests the intercalation of **10** into the DNA in agreement with both binding data and fluorescence titration.

Cell uptake studies: Due to a lack of reasonable DNA binding of ligand **4** and complex **9**, we focused our in vitro studies on ligand **7** and complex **10**. We selected two different cell lines for these studies, a B16-F1 mouse melanoma cell line with no expression of the GRP receptor and a human prostate adenocarcinoma cell line, PC-3, which does express the GRP receptor.[28] The latter cell line can be used for targeting studies with the BBN derivative **13**. The uptake of

complex **10** was detected in the green fluorescence filter ($\lambda_{em} = 530$ nm) as described in the Experimental Section. To localize the uptake in the cell, we stained nuclei with DAPI (4′,6-diamidino-2-phenylindol), routinely used in cell biology. After exposing the cells to DAPI and **10** (50 μM) for 2 h, both B16-F1 and PC-3 cells were readily loaded with complex **10** as detected by fluorescence microscopy and depicted in Figure 6.

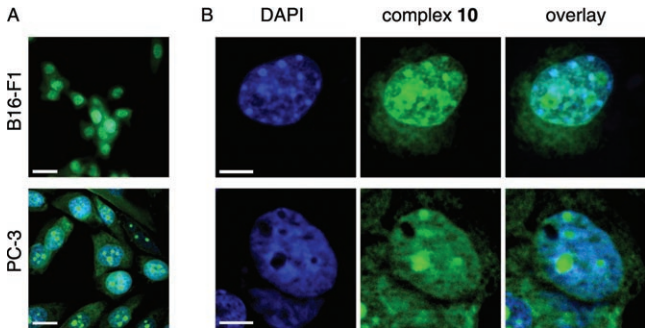

Figure 6. Uptake of the complex **10** by B16-F1 and PC-3 cells was evaluated by immunofluorescence microscopy. Cells were incubated with 100 μM complex **10** for 1 h followed by fixation of cells and nuclear staining by DAPI. A) Overview images of B16-F1 cells showed uptake of **10** in the cytoplasm (green) with a profound accumulation in the cell nuclei (blue colour), as visualized by a green staining along with DAPI (light blue colour). PC-3 cells were also loaded with **10** in the cytoplasm (green), with accumulation in the nuclei. Note the profound concentration of **10** found in the nucleoli (bar = 20 μm). B) High-magnification images of individual cells, where the localization of **10** in the nucleus is visible. Single channel images of the cell for DAPI staining (blue) and for **10** staining (green) were co-localized in the merged image (overlay). Images represent stacks of optical sections from the cell taken over 3 μm (z section; bar = 10 μm).

The cationic complex **10** rapidly accumulates in the cell nuclei, despite of the bulky pendant metal complex (Figure 6). Both cells, B16-F1 and PC-3, were loaded efficiently with complex **10** as detected by a staining of the cytoplasm. The diverse biological background of the cells did not play a role by the uptake, thus indicating that **10** could be considered as a nuclear-targeting agent. Interestingly, complex **10** was accumulated in the nucleoli of PC-3 cells, in particular. This observation correlated with the earlier findings for europium complex nucleoli targeting.[8] The tight binding of **10** to DNA was nicely visualized in dividing PC-3 cells (Figure 7). The clear recognition of chromosomes centrally organized in a dividing cell during anaphase co-localized with **10** bound to the DNA (green). The pronounced accumulation/association of complex **10** with the nuclear DNA of dividing cells makes this compound of interest for treatment of cancer, in which the dividing tumour cells are the primary targets of therapy. However, the proof of principle for nuclear targeting with **10** requires guarantee for the cell specificity, which could be addressed through tumour-specific receptors like GRP.

Specific cell targeting: The observation that complex **10** readily accumulated in the nucleus indicates that this complex effectively crosses the cell membrane. It is unlikely that the entrance of this complex is mediated by endocytosis. Previous findings have shown that the uptake of a europium complex by cells occurred also at 4 °C, thereby excluding an active transport mechanism from this process.[8] To test the specificity of specific cell targeting with complexes based on **10**, the GRP receptor-specific peptide, Bombesin, is conjugated in complex **13**.

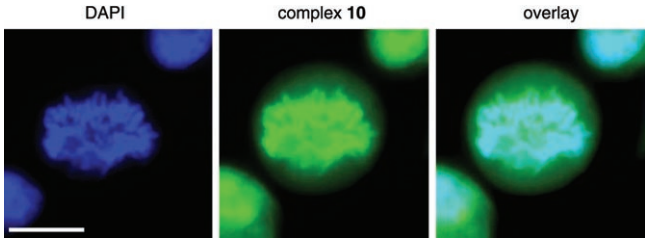

Figure 7. Complex **10** binding to the nuclear DNA of PC-3 cells during cell division. DAPI staining shows the centrally organized chromosomes "fingers", pointing out the early anaphase of the cell cycle. The dominant complex **10** staining (green) is co-localized with the DAPI staining as could be appreciated by the light blue colour, indicating co-localization (overlay). Cells during division have a rounded shape, thus causing a slight "blurry" image of the surrounding cytoplasm (bar = 10 μm).

The trifunctional compound **13** was synthesized as outlined above. Compound **13** was purified by preparative HPLC and tested for stability in buffered aqueous solutions. The complex is stable for at least 24 h and the ligand **7** does not cleave from the complex. Compound **13** was added to B16-F1 and PC-3 cells at concentrations of 100 μM and incubated for 2 h. Cells were evaluated by immunofluorescence microscopy (Figure 8).

While there was virtually no uptake of compound **13** in B16-F1 cells, PC-3 cells were readily loaded with **13** in the cytoplasm. In contrast to complex **10**, the uptake of **13** by the cells was significantly suppressed in B16-F1 cells, indicating that this peptide-bound metal complex could not cross the cell membrane anymore. The significant uptake of compound **13** by PC-3 cells was consistent with the presence

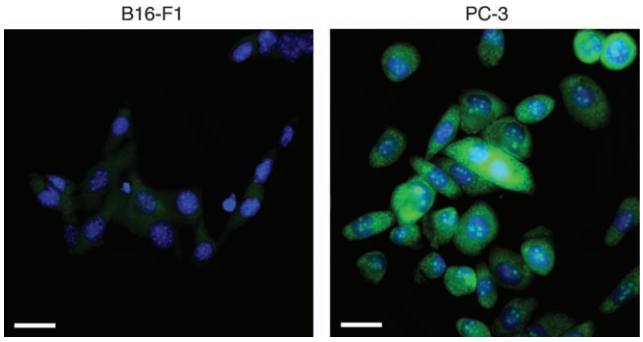

Figure 8. Cells were incubated with 100 μM of compound **13** for 2 h, followed by fixation and nuclear staining with DAPI as described in the Experimental Section. B16-F1 cells showed very little of the compound as determined by almost background level green fluorescence in the cytoplasm. PC-3 cells were robustly loaded in the cytoplasm by a green fluorescence (bar = 20 μm).

of the GRP receptor by these cells, thus indicating a receptor-mediated active uptake. As can be clearly seen in Figure 8, no uptake into the nucleus takes place. Cell-specific nuclear targeting requires cleavage of the peptide from the metal complex in order to set free the active nuclear-targeting functions. This is feasible by the introduction, for example, of pH sensitive cleavable linkers between peptide and complex. The low pH in the lysosomes would then induce the release, for example, of complex **10** from **13**. Fast and localized activation of a drug from a prodrug is a well-known challenge in pharmaceutical chemistry and requires further investigations in the context of metal complexes.

^{99m}Tc-labelling studies: The precursor $[^{99m}Tc(OH_2)_3(CO)_3]^+$ was prepared from $[^{99m}TcO_4]^-$ by using the Isolink kit (Mallinckrodt Med. B.V. Petten, NL).[29,30] The concentration of ^{99m}Tc is in the range of 10^{-7} M. After kit preparation, the solution was buffered with 0.1 M phosphate buffer to pH 7.4 before further reaction. HPLC analyses with γ-detection were performed to quantify the conversion of the ^{99m}Tc. Reaction time, concentrations and temperature were varied. Typical labelling yields are given in Table 2.

Table 2. Yields and reaction conditions for the conversion of $[^{99m}Tc(OH_2)_3(CO)_3]^+$ to $[^{99m}Tc(L^2)(L^1)(CO)_3]^+$.

$[Tc(OH_2)(CO_3)_3(L^2)]$/ $[Tc(L^1)(CO_3)_3(L^2)]$	complex	*t* [min]	*T* [°C]	$[L^2/L^1]$ [mM]	Yield [%]
2,4-pydic/**4**	**14/16**	40/60	75/80	0.1	>98/95
2,4-pydic/**7**	**14/17**	40	75/90	0.1	>98/90
2,4-pydic-BBN (**11**)/**7**	**15/18**	60	80/90	0.1	95/95

The [2+1] mixed ligand synthesis of complexes of the general type $[^{99m}Tc(CO)_3(L^2)(L^1)]$ consists of two consecutive steps.[16] First, $[^{99m}Tc(OH_2)_3(CO)_3]^+$ reacts with a bidentate ligand L^2. Then, the monodentate ligand L^1 is coordinated to the sixth available coordination site on the *fac*-$[^{99m}Tc(CO)_3]^+$ core by replacing the remaining water ligand. For example, reactions of $[^{99m}Tc(OH_2)_3(CO)_3]^+$ with the L^2 ligands 2,4-pydic or the BBN conjugate **11** gave $[^{99m}Tc(OH_2)$(2,4-pydic)$(CO)_3]$ (**14**) and ^{99m}Tc-labelled BBN $[^{99m}Tc(OH_2)(\mathbf{11})(CO)_3]$ (**15**), respectively, in near quantitative yield. Reaction conditions are 30–60 min at 70 °C and L^2 concentrations are 10^{-4} M. Concentrations of 10^{-5} M are possible without significant decrease of the yield. It should be noted that no coordination of a second ligand was observed.

In the subsequent step, the monodentate nuclear-targeting ligands **4** and **7** were introduced. This reaction is significantly slower and higher temperatures are required to bring the reaction to completion within 60 min. Reaction of **14** with the acridine derivative **4** gave the radiolabelled complex $[^{99m}Tc(\mathbf{4})$(2,4-pydic)$(CO)_3]$ (**16**), and with the acridine orange compound **7** the cationic complex $[^{99m}Tc(\mathbf{7})$(2,4-pydic)$(CO)_3]^+$ (**17**). Complex **17** is the homologue of **10** used in the previous fluorescence studies. Finally, reaction of **15** with **7** gave the radioactive trifunctional complex $[^{99m}Tc(\mathbf{7})(\mathbf{11})(CO)_3]$ (**18**), the homologue of **13**. Yields and reaction conditions are given in Table 2.

Due to the very low concentrations the ^{99m}Tc complexes ($\approx 10^{-7}$ M), common analytical methods such as NMR or UV/Vis spectroscopy or mass spectrometry cannot be applied for characterization of the complexes. Usually, characterization is performed by comparing the HPLC traces of the ^{99m}Tc compounds with the fully characterized rhenium analogues. Equal retention times of the radioactive trace recorded with γ detection and the UV/Vis trace of the rhenium complex indicates identical complexes.

The reaction of $[^{99m}Tc(OH_2)_3(CO)_3]^+$ with 2,4-pydic gives **14**. Retention time of **14** is 19.5 min which compares well with that of the rhenium analogue **8** (18.8 min). Adding ligand **4** to **14** gives the neutral complex **16**, which is more lipophilic and longer retention times are observed correspondingly. Again, authenticity of **16** is confirmed by comparing the retention times for **16** (24.5 min) which is equal to that of the rhenium analogue **9** (23.9 min).

At a ligand (**7**) concentration of 10^{-4} M, **14** was quantitatively labelled at 90 °C after 40 min to provide the product **17**. Compound **17** display a similar HPLC pattern as **13** with retention times of 23.7 and 23.2 min, respectively.

The reaction of the derivatised bombesin **11** with $[^{99m}Tc(OH_2)_3(CO)_3]^+$ at 80 °C gave $[^{99m}Tc(OH_2)$(2,4-pydic-BBN)$(CO)_3]$ (**15**) in good yield after 60 min . The two peaks at 13.73 and 14.10 min represent the expected diastereomers. The identity of the peaks was confirmed by comparison with $[Re(OH_2)(\mathbf{11})(CO)_3]$. The introduction of ligand **7** leads to the formation of the positively charged complex **18**. While two peaks are observed in the HPLC trace of complex **15**, corresponding to two diastereomers, only one peak is visible in the case of **18**. This implies that only the thermodynamically more favoured diastereomer is formed or that the two forms can not be separated under HPLC conditions. The small peaks at 14.10 and 13.73 min are unreacted **15** (Figure 9).

Histidine and cysteine challenge: The stabilities of the labelled compounds **16**, **17** and **18** were challenged with the

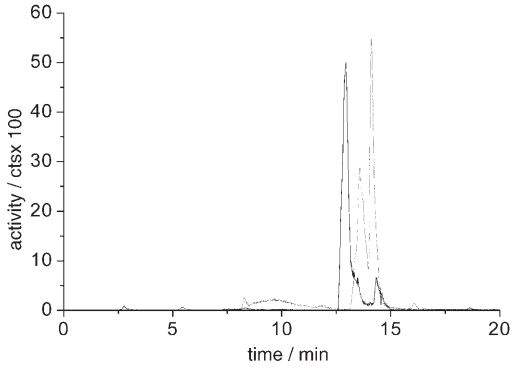

Figure 9. Radioactive HPLC trace of **15** (dotted line). Formation of the final compound **18** (solid line); Linear gradient: ammonium acetate/acetonitrile (90:10) to 100% acetonitrile from 10 to 20 min and then back to ammonium acetate/acetonitrile (90:10). The flow rate was 1.5 mL min^{-1}.

very potent tridentate ligands histidine and cysteine at a molar ratio of 1/100. The mixtures were kept at 37 °C, pH 7 for 2, 4 and 12 h. Analysis by HPLC revealed complete stability of the ^{99m}Tc complexes under these conditions. Besides the intact radiolabelled complexes, no $^{99m}TcO_4^-$ could be observed. The stability study of these complexes showed that no significant ligand exchange and/or decomposition are expected within 12 h of incubation.

Conclusion

We have shown the individual steps required for targeting the nucleus of a specific cell type with rhenium and with ^{99m}Tc. A bifunctional nucleus-targeting molecule is able to carry a metal complex into its target. A trifunctional molecule, which contains, in addition, receptor-specific bombesin, is only taken up by cells containing the GRP receptor. These two decisive steps have now to be followed by the study of trifunctional molecules containing a pH-dependent cleavable linker between the nucleus-targeting metal complex and the cell-targeting peptide. These studies are currently underway.

Experimental Section

General information: All solvents were of the quality puriss or p.a. The commercially available reagents were used as received without further purification. Analytical thin-layer chromatography (TLC) was carried out by using aluminium-based plates (silica gel 60 F254) from Merck. Plates were visualized under UV light ($\lambda = 254$ nm). Flash chromatography was carried out by using Merck silica gel 60 (0.040–0.063 mm) with N_2 overpressure. Samples were applied as almost saturated solutions in the appropriate solvent. ^{1}H NMR and ^{13}C NMR spectra were performed on a Varian Gemini 300 and Bruker DRX500 spectrometers at 300 and 75 MHz, and 500 and 125 MHz respectively. The reported chemical shifts (in δ) are relative to the solvent protons and carbons as a reference. Multiplicities are reported using the following abbreviations: s (singlet), d (doublet), t (triplet) and m (multiplet). IR spectra of solids were recorded on a Bio-Rad FTS-45 spectrometer with samples in compressed KBr-pellets. Mass spectra were measured on a Merck Hitachi M-8000 spectrometer. Linear dichroism (LD) measurements were performed with a Jasco J500 A spectropolarimeter equipped with an IBM PC and a Jasco J interface. The sample orientation was produced by a device designed by Wada and Kozawa for the studies of differential flow dichroism of polymer solution at a shear gradient of 700 rpm in phosphate buffer 10 mM pH 7.2.[31] High-performance liquid chromatography (HPLC) was performed on a Merck L7000 system by using a Macherey-Nagel EC 250/3 Nucleosil 100–5 C18HD column. HPLC solvents were 0.1% trifluoroacetic acid as solvent A and methanol as solvent B. The flow rate was 0.5 mL min^{-1}. Detection was performed at 250 nm. Preparative HPLC was performed on a Varian Pro Star system by using either a Macherey-Nagel VP 250/21 Nucleosil 100–7 C18 or a Macherey-Nagel VP 250/40 Nucleosil 100–7 C18 column with a flow rate of 10 mL min^{-1} and 40 mL min^{-1}. respectively. The solvents were 0.1% trifluoroacetic acid as solvent A and methanol as solvent B. The gradient used for analysis was : 0–3 min 100% A, 3.1–9 min 75% A, 9.1–20 min 66% to 0% A, 20–25 min 0% A, 25.1–30 min 100% A. All ITC measurements were carried out on a MicroCal VP-ITC microcalorimeter at pH 7.0 and 37 ($\pm$ 0.01) °C. The cell volume was 1.406 mL and the syringe volume had a maximum capacity of 267 µL. All samples were prepared in a 1 mM sodium cacodylate buffer at pH 7.0 and degassed before the measurements. To avoid a π–π stacking of the acridine orange residues, a low concentration of 0.3 mM of **7** and 0.5 mM of **10** was chosen. The concentration of the ct DNA was 0.07 mM in the titration with **7** and 0.04 mM for **10**. The raw heat–flow versus time data was baseline adjusted, peak integrated, and processed with the Origin Software Package version 7.0 and the corresponding VP Viewer 2000 ITC to obtain the molar heat flow per molar ratio. $\Delta G_{overall}$, the free energy of each ITC titration, was calculated from integrated experimental data of the equilibrium constant K_{ITC}. The sequential binding model fit with three sequential binding sites was chosen to fit the experimental data.

Cell culture and complex uptake: B16-F1 mouse melanoma cells were cultured in DMEM supplemented with 10% fetal calf serum. Human prostate cancer cells, PC-3 were incubated in F12K medium supplemented with 10% fetal calf serum. For microscopy, cells were cultured overnight on 4-chamber slides (Nunc) in which $\approx$50000 cells were plated. Next day, cells were washed and fresh medium containing complex **10** or **13** (100 µM) was added. Cells were incubated with the complex for 1–2 h. After the loading with a complex, cells were washed with phosphate buffer saline (PBS) and fixed in 3% paraformaldehyde for 10 min in at RT. After three washings with PBS, cells were incubated in 1 µg mL^{-1} 4′,6-diamidino-2-phenylindole (DAPI) for nuclear staining for 10 min at RT. Cells were washed three times with phosphate-buffered saline (PBS), chambers from the slides were detached and cells were covered with coverslips in Prolong Mounting medium (Invitrogen). Slides were evaluated on Zeiss Axiovert 200 M with the corresponding fluorescence filters for DAPI (λ_{ex}=360 nm, λ_{em}=420 nm) and acridine orange (λ_{ex}=496 nm, λ_{em}=525 nm). In some cases optical sectioning with Apotom system (Zeiss) was performed

Acridine-4-carboxylic acid (1): The synthesis was performed according to literature with modifications.[32] Portions (100–200 mg each) of Al foil (1.7 g, 0.063 mol) were amalgamated with Hg by immersing them for 1 min in a solution of mercuric chloride (6.0 g, 0.022 mol) in ethanol (50 mL),. After being washed in ethanol, these were added over 20 min to a refluxing, stirred solution of 9-oxiacridan-4-carboxylic acid (2.0 g, 0.0083 mol) dissolved in 50% aqueous ethanol (15 mL) containing KOH (530 mg, 0.009 mol). When the reaction was complete, as indicated by HPLC, 1 M aqueous KOH (36 mL) was added, the hot mixture was filtered and the solids were washed with hot 50% aqueous ethanol (15 mL). The combined filtrates were strongly acidified with 12 M HCl, treated with $FeCl_3$ (500 mg, 0.003 mol), heated under reflux until homogeneous, and clarified by filtration. Solid $K(O_2CCH_3)$ was then added to just complete precipitation of the crude product, which was immediately collected by filtration and washed well with water. It was then dissolved in dilute aqueous KOH, filtered, diluted while hot with ethanol and then treated slowly with acetic acid, when acridine-4-carboxylic acid separated as a pale yellow solid (1120 mg, 61%), suitable for further use. ^{1}H NMR (500 MHz, [D$_4$]CD$_3$OD): δ = 9.35 (s, 1H), 8.83 (d, ^3J(H,H) = 7.6 Hz, 1H), 8.47 (d, ^3J(H,H) = 9.1 Hz, 1H), 8.26–8.23 (t, ^3J(H,H) = 8.5 Hz, 2H), 8.13 (d, ^3J(H,H) = 9.0 Hz, 1H), 7.82–7.79 (t, ^3J(H,H) = 9.0 Hz, 1H), 7.76–7.73 ppm (t, ^3J(H,H) = 8.3 Hz, 1H); ^{13}C NMR (75 MHz , [D$_4$]CD$_3$OD): δ = 168.3, 148.5, 144.9, 139.2, 135.7, 134.2, 132.7, 129.6, 129.4, 127.7, 127.5, 126.3, 125.9, 125.2 ppm; IR (KBr): $\tilde{\nu}$ = 1703 (s), 1623 (s), 1569 (s) 1516 (s), 1427 (m), 739 cm^{-1} (s); HPLC: R_t: 18.4 min; ESI-MS : m/z: 224.00 $[M+H]^+$; elemental analysis (%) calcd for $C_{14}H_9NO_2$: C 75.33, H 4.06, N 6.27; found: C 75.72, H 3.99, N 5.82.

Acridine-4-carboxylic acid (2-aminoethyl)amide (2): A suspension of acridinecarboxylic acid (580 mg, 2.190 mmol) and (benzotriazol-1-yloxy)-tris(dimethylamino)phosphonium hexafluorophosphate (BOP; 3.48 g, 7.86 mmol) in dichloromethane (25 mL) was stirred for 2 h at RT. The reaction mixture was cooled at 0 °C, ethylenediamine (1.3 mg, 21 mmol) was added dropwise and the resulting reaction mixture was stirred for another 3 h at RT. The solvent was removed in vacuo and the crude product was purified by flash chromatography (silica gel, CH_2Cl_2/MeOH/NH_4OH-25%, 10:1:0.1, R_f = 0.34) to give **2** (326 mg, 56%) as a yellow oil. ^{1}H NMR (500 MHz, [D$_4$]CD$_3$OD): δ = 8.64 (s, 1H), 8.14 (d, ^3J(H,H) = 8.1 Hz, 1H), 7.90–7.74 (m, 4H), 7.53–7.45 (dd, ^3J(H,H) = 9.3, ^4J(H,H) = 2.4 Hz, 2H), 3.62 (t, ^3J(H,H) = 9.6 Hz, 2H), 3.33 (br s, 2H), 2.97 ppm (t, ^3J(H,H) = 9.6 Hz, 2H); ^{13}C NMR (125 MHz, [D$_4$]CD$_3$OD): δ = 169.1,

149.2, 147.3, 139.8, 136.1, 134.7, 133.2, 129.9, 129.4, 128.4, 127.9, 126.3, 125.6, 42.1, 37.4 ppm; HPLC: R_t: 19.45 min; ESI-MS : m/z: 265.53 $[M+H]^+$; elemental analysis (%) calcd for $C_{16}H_{15}N_3O$: C 72.43, H 5.70, N 15.84; found: C 73.82, H 5.65, N 13.22.

Acridine-4-carboxylic acid (2-formylaminoethyl)amide (3): Compound **2** (326 mg, 1.23 mmol) was suspended in methyl formate (10 mL). This mixture was refluxed for 3 h, under exclusion of air. After addition of *p*-toluylsulfonic acid (7 mg) the reaction mixture was refluxed for another 14 h (HPLC-control). The solvent was removed in vacuo and the crude product purified by flash chromatography (silica gel, CH_2Cl_2/MeOH/NH_4OH-25%, 10:1:0.1, $R_f=0.45$) to give 283 mg (79%) of **3** as a yellow powder. ^{1}H NMR (300 MHz, [D$_4$]CD$_3$OD): $\delta=8.64$ (s, 1H), 8.14 (d, ^3J(H,H)=8.3 MHz, 1H), 8.10 (s, 1H), 7.90–7.74 (m, 4H), 7.53–7.45 (dd, ^3J(H,H)=8.4, ^4J(H,H)=2.5 Hz, 2H), 3.62 (t, ^3J(H,H)=9.1 Hz, 2H), 3.33 (br s, 1H), 2.97 ppm (t, ^3J(H,H)=8.9 Hz, 2H); ^{13}C NMR (75 MHz, [D$_4$]CD$_3$OD): $\delta=168.3$, 163.2, 148.5, 139.2, 135.7, 134.2, 132.7, 129.6, 129.4, 127.5, 125.9, 125.2, 43.4, 42.2 ppm; HPLC: R_t: 19.8 min; ESI-MS: m/z: 293.73 $[M+H]^+$; elemental analysis (%) calcd for $C_{17}H_{15}N_3O_2$: C 69.61, H 5.15, N 14.33; found: C 69.29, H 5.25, N 14.55.

Acridine-4-carboxylic acid (2-isocyanoethyl)amide (4): Ethylentriamine (270 mg, 2.70 mmol) was added to a solution of **3** (258 mg, 0.880 mmol) in absolute dichlormethane (10 mL). The mixture was cooled to 0°C and phosphorusoxychloride ($POCl_3$; 148.5 mg, 0.970 mmol) was added dropwise. After 2 h reaction time a solution of sodium carbonate (Na_2CO_3, 164 mg) in water (1 mL) was added. The reaction mixture was stirred for 1 h at RT. The resulting suspension was then treated with water (10 mL; till clear) and extracted three times with $CHCl_3$. The organic layer was dried over Na_2SO_4 and the solvent was removed in vacuo. The crude product was purified by flash chromatography (silica gel, CH_2Cl_2/MeOH, 10:0.5, $R_f=0.43$) to give **4** (70 mg, 29%) as a yellow powder. ^{1}H NMR (300 MHz, [D$_4$]CD$_3$OD): $\delta=8.64$ (s, 1H), 8.14 (d, ^3J(H,H)=8.1 Hz, 1H), 7.90–7.74 (m, 4H), 7.53–7.45 (dd, ^3J(H,H)=8.7, ^4J(H,H)=2.8 Hz, 2H), 3.62 (t, ^3J(H,H)=8.7 Hz, 2H), 2.97 ppm (t, ^3J(H,H)=9.2 Hz, 2H); ^{13}C NMR (75 MHz, [D$_4$]CD$_3$OD): $\delta=168.3$, 157.2, 148.5, 139.2, 135.7, 134.2, 132.7, 129.6, 129.4, 127.5, 125.9, 125.2, 44.4, 43.2 ppm; IR (KBr): $\tilde{\nu}=3053$ (w), 2150 (m), 1659 (s), 1624 (m), 1566 (m), 910 (w), 737 cm^{-1} (m); HPLC: R_t: 21.4 min; ESI-MS: m/z: 275 $[M+H]^+$; elemental analysis (%) calcd for $C_{17}H_{13}N_3O$: C 74.17, H 4.76, N 15.26; found: C 73.92, H 4.87, N 15.11.

3,6-Bis-dimethylamino-10-(4-formylaminobutyl)acridinium (6): A solution of **5** (250 mg, 0.943 mmol) and 4-bromobutyl formamide (340 mg, 1.886 mmol) in p-xylene (20 mL) was stirred, under N_2, for 24 h at 145°C. The solvent was removed in vacuo and the crude product was purified by flash chromatography (basic alox, CH_2Cl_2/MeOH, 5:2, $R_f=0.33$) to give **6** (179 mg, 52%) as an dark orange powder. ^{1}H NMR (500 MHz, [D$_4$]CD$_3$OD): $\delta=8.93$ (s, 1H), 8.2 (s, 1H), 7.85 (d, ^3J(H,H)=9.3 Hz, 2H), 7.20 (dd, ^3J(H,H)=9.2, ^4J(H,H)=2.1 Hz, 2H), 6.74 (s, 2H), 4.67 (t, ^3J(H,H)=7.7 Hz, 2H), 3.56 (s, 12H), 3.21 (s, 2H), 2.99 ppm (m, 4H); ^{13}C NMR (125 MHz, [D$_4$]CD$_3$OD): $\delta=164.5$, 157.4, 144.3, 144.0, 134.4, 134.0, 122.9, 121.1, 115.0, 93.7 (4C), 71.1, 61.9, 41.2 (4C), 40.5, 25.7, 24.2 ppm; IR (KBr): $\tilde{\nu}=1691$ cm^{-1} (s); ESI-MS: m/z: 365.27 $[M+H]^+$.

3,6-Bis-dimethylamino-10-(4-isocyanobutyl)acridinium (7): A mixture of **6** (100 mg, 0.274 mmol) and diisopropylamine (222 mg, 2.2 mmol) in dichloromethane (10 mL) was cooled to −8°C and stirred for half hour. $POCl_3$ (168 mg, 1.1 mmol) was added over a period of 10 min, followed by stirring at the same temperature for six hours. The reaction mixture was quenched by cautious addition of an aqueous solution of sodium carbonate (20%, 2.3 mL). After stirring at ambient temperature for one hour, water (2 mL) and dichloromethane (1 mL) were added. The organic phase was separated and washed with water (3×1 mL). The aqueous phases were extracted with dichloromethane (3×2 mL) and the combined organic solutions were dried over sodium sulfate. Evaporation of the solvent gave the crude product as an orange powder. The crude product was purified by flash chromatography (basic alox, CH_2Cl_2/MeOH/NH4OH-25%, 10:1:0.1, $R_f=0.38$) to give **7** (51 mg, 54%) as an orange powder. ^{1}H NMR (500 MHz, [D$_4$]CD$_3$OD): $\delta=8.71$ (s, 1H), 7.95 (d, ^3J(H,H)=8.3 Hz, 2H), 7.32 (dd, ^3J(H,H)=9.2, ^4J(H,H)=2.1 Hz, 2H), 6.74 (s, 2H), 4.80 (t, ^3J(H,H)=8.2 Hz, 2H), 3.32 (s, 12H), 2.21–2.15 (m, 2H), 2.04 (br s, 2H), 1.28 ppm (s, 2H); ^{13}C NMR (125 MHz, [D$_4$]CD$_3$OD): $\delta=157.7$, 144.7, 144.4, 134.6, 118.8, 115.8, 93.7, 47.7, 42.12, 41.03, 27.6, 23.8 ppm; IR (KBr): $\tilde{\nu}=2145$ (w), 1608 (s), 1522 (m), 1504 (m), 1363 (m), 1165 (m), 806 cm^{-1} (w); HPLC: R_t: 20.7 min; ESI-MS: m/z: 347.13 $[M+H]^+$; elemental analysis (%) calcd for $C_{22}H_{27}N_4$: C 62.30, H 6.42, N 13.20; found: C 61.10, H 6.54, N 12.97.

[Re(OH$_2$)(2,4-pydic)(CO)$_3$] (8): $(NEt_4)_2[ReBr_3(CO)_3]$ (101 mg, 0.13 mmol) was dissolved in water (2 mL). After addition of $AgNO_3$ (70 mg, 0.4 mmol) and stirring at RT for 3 h, AgBr was removed by filtration and 2,4-pydic (24 mg, 0.13 mmol) was added to the colourless solution, which contained $[Re(OH_2)_3(CO)_3]^+$, followed by stirring at 50°C for 2 h. The now yellow solution was cooled down and the product was allowed to crystallize at 4°C for 12 h. The yellow crystals were collected by filtration, washed with water and dried at high vacuum to give **8** (36 mg, 62%). ^{1}H NMR (300 MHz, [D$_6$]DMSO): $\delta=8.96$ (d, ^3J(H,H)=9.0 Hz, 1H), 8.34 (d, ^3J(H,H)=8.1 Hz, 1H), 8.15 (d, ^3J(H,H)=8.6 Hz, 1H), 7.50 ppm (s, 1H); ^{13}C NMR (75 MHz, [D$_6$] DMSO): $\delta=197.8$, 194.4, 174.5, 165.6, 154.5, 153.8, 143.2, 133.2, 128.4 ppm; IR (KBr): $\tilde{\nu}=$ 2023 (s), 1892 (s), 1717 (w), 1646 (m), 1611 (m), 1374 (w), 1348 (w), 770 cm^{-1} (w); HPLC: R_t: 17.8 min; ESI-MS: m/z: 437.60 $[M-OH_2]^+$; elemental analysis (%) calcd for $C_{10}H_6NO_8Re$: C 26.45, H 1.33, N 3.07; found: C 26.15, H 1.67, N 3.07.

[Re(4)(2,4-pydic)(CO)$_3$] (9): A solution of **8** (29 mg, 0.064 mmol) and **4** (17.5 mg, 0.064 mmol) in methanol (2 mL) was stirred at room temperature for 12 h. HPLC analysis showed complete product formation. The solvent was removed in vacuo and the crude product was purified by preparative HPLC to give **9** as yellow powder in a yield of (36 mg, 80%). Crystals for X-ray diffraction analysis were obtained by slow evaporation of a solution of **9** in methanol/dichloromethane (1:1). ^{1}H NMR (500 MHz, [D$_4$]CD$_3$OD): $\delta=9.15$ (s, 1H), 8.63 (dd, ^3J(H,H)=7.1, ^4J(H,H)=1.5 Hz, 1H), 8.35 (d, ^3J(H,H)=6.5 Hz, 1H), 8.33 (dd, ^3J(H,H)=8.4, ^4J(H,H)=1.0 Hz, 1H), 8.26 (d, ^3J(H,H)=8.3 Hz, 1H), 8.20 (d, ^3J(H,H)=8.3 Hz, 2H), 7.94 (m, 1H), 7.71 (m, 2H), 7.54 (dd, ^3J(H,H)=6.5, ^4J(H,H)=1.8 Hz, 1H), 4.22 (s, 2H), 3.91 ppm (m, 2H); ^{13}C NMR (125 MHz, [D$_4$]CD$_3$OD): $\delta=193.5$, 193.2, 191.0, 174.3, 168.8, 168.1, 163.3, 163.0, 154.3, 151.6, 149.2 148.1, 147.2, 138.4, 136.6, 135.2, 133.3, 130.1, 129.7, 129.0, 128.4, 127.4, 126.3, 119.5, 117.2, 48.6, 39.7 ppm; IR (KBr): $\tilde{\nu}=2212$ (w), 2033 (s), 1946 (s), 1908 (s), 1647 (s), 1381 cm^{-1} (w); HPLC: R_t: 20.8 min; ESI-MS: m/z: 692.53 $[M-OH]^+$.

[Re(7)(2,4-pydic)(CO)$_3$] (10): A solution of **8** (9 mg, 0.020 mmol) and **7** (7 mg, 0.020 mmol) in methanol/water (2 mL; 1:1) was stirred at 75°C for 2 h. HPLC analysis showed complete product formation. The solvent was removed in vacuo and the product was dried at high vacuum. The crude product was purified by flash chromatography (basic Alox, CH_2Cl_2/MeOH/NH_4OH, 5:0.7, 0.05 $R_f=0.29$). Product **10** (9 mg, 65%) was obtained as an dark orange powder. Crystals for X-ray diffraction analysis were obtained by slow evaporation of a solution of **10** in methanol/dichloromethane (1:1). ^{1}H NMR (700 MHz, [D$_4$]CD$_3$OD): $\delta=8.72$ (d, ^3J(H,H)=6.3 Hz, 1H), 8.67 (s, 1H), 8.63 (s, 1H), 8.34 (s, 1H), 8.11 (s, 1H), 7.93–7.88 (m, 1H), 7.29–7.26 (m, 1H), 6.68 (s, 1H), 6.53 (s, 1H), 4.75 (t, ^3J(H,H)=7.8 Hz, 2H), 3.95 (s, 2H), 3.35 (s, 12H), 2.21–2.15 (m, 2H), 2.04 (br s, 2H), 1.30 ppm (s, 2H); ^{13}C NMR (175 MHz, [D$_4$]CD$_3$OD): $\delta=192.9$, 192.7, 190.3, 173.6, 168.5, 163.2, 156.6, 153.5, 150.5, 150.3, 143.8, 143.5, 143.2, 140.1, 133.4, 133.6, 128.5, 126.7, 117.7, 117.5, 114.7, 92.8, 92.4, 47.3, 46.8, 46.0; 44.2, 40.1, 37.5, 27.3, 26.5, 23.5 ppm; IR (KBr): $\tilde{\nu}=2212$ (w) 2028 (m), 1946 (m), 1907 (m), 1643 (m), 1600 (s), 1503 (m), 1365 (s), 1168 (s), 805 cm^{-1} (w); HPLC: R_t: 21.8 min; ESI-MS: m/z: 783.43 $[M+H]^+$, 754.87 $[M-CO]^+$.

Peptide synthesis: Bombesin (sequence: WAVGHLM) was synthesized on an Applied Biosystems ABI433 A peptide synthesiser by using standard Fmoc chemistry and Rink amide MBHA resin (360 mg, 0.66 mmol/g). The following side-chain protected amino acids were used for the synthesis: Fmoc-Ala-OH, Fmoc-Gln(Trp)-OH, Fmoc-Gly-OH, Fmoc-His(Trt)-OH, Fmoc-Leu-OH, Fmoc-Met-OH Fmoc-Trp(Boc)-OH and Fmoc-Val-OH. Fmoc deprotection was performed by using 20% piperidine in *N*-methylpirrolidone (NMP). Coupling reactions were carried out by using 2-(1*H*-benzotriazole-1-yl)-1,1,3,3,-tetramethylaminium hexafluorophosphate/N-hydroxy-benzotiazole (HBTU/HOBt) (4 equiv) with

diisopropylethylamine (DIEA) (8 equiv). At the end of the synthesis, the peptide was cleaved from the solid-support and deprotected by shaking the resin in trifluoroacetic acid/water/triisopropylsilane (95:2.5:2.5 15 mL) for 3 h. The resin was removed by filtration, and after concentration in vacuo, the crude deprotected peptide was precipitated by addition of cold iPr$_2$O (5 mL). After centrifugation, the pellet was washed twice with iPr$_2$O and dried under high vacuum. The product was then purified by reverse phase HPLC on a preparative C_{18} column (Zorbax Eclipse XDB-C18; 21 mm×250 mm, 7 μm, 80 Å) using a gradient of 5 to 50% acetonitrile in water (+ 0.1% TFA) over 15 min and a flow of 15 mL min^{-1}. HPLC: R_t: 14.5 min; ESI/MS: m/z: 812.7 $[M+H]^+$.

Pyridine-2,4-dicarboxylic acid 2-methyl ester bombesin: A solution of pyridine-2,4-dicarboxylic acid-2-methylester (5.4 mg, 0.0296 mmol) in DMF (0.5 mL) and BOP (26 mg, 0.0591 mmol) was stirred for 3 h at 0 °C. Then a solution of BBN (18 mg, 0.0197 mmol) and triethylamine (TEA; 18 mg, 0.0597 mmol) in DMF (1 mL) was slowly added. The reaction mixture was stirred for 3 h at 0 °C and 1 h at room temperature. The solvent was removed in vacuo and the crude product was purified by flash chromatography (silica gel, CH_2Cl_2/MeOH/NH_4OH-25%, 5:1:0.1 R_f= 0.08). The product (20 mg, 83%) was obtained as a white powder. HPLC: R_t: 20.35 min; ESI-MS: m/z: 975.83 $[M+H]^+$.

2,4-Pyridine-dicarboxylic acid bombesin (2,4-Pydic–BN; 11): NaOH (0.1 M, 8.0 mg, 0.200 mmol) was added to a solution of pyridine-2,4-dicarboxylic acid 2-methyl ester bombesin (20 mg, 0.020 mmol) in DMF (1 mL). The resulting colourless solution was stirred for 1 h at 0 °C and for another hour at room temperature. The solvent was removed in vacuo and the product was purified by preparative HPLC to give **11** (8 mg, 41%) as a white powder. HPLC: R_t: 19.7 min; ESI-MS: m/z: 961.51 $[M+H]^+$.

[Re(OH$_2$)(11)(CO)$_3$] (12): Compound **7** (1.4 mg, 0.0042 mmol) was added to a solution of **11** (4 mg, 0.0042 mmol) in methanol (2 mL). The resulting colourless solution was stirred for 1 h at room temperature and for another hour at 80 °C. HPLC analysis showed complete product formation. The solvent was removed in vacuo and the product was dried at high vacuum to give **12** (5 mg, 92%) as white powder. HPLC: R_t: 20.3 min; ESI-MS: m/z: 1230.93 $[M-OH_2]^+$.

[Re(7)(11)(CO)$_3$] (13): Compounds **12** (5 mg, 0.0057 mmol) and **7** (2 mg, 0.0057 mmol) in water/methanol (8 mL; 1:1). The orange solution was stirred for 3 h at 85 °C. The ESI-MS and HPLC analysis confirmed the disappearance of **7** and the formation of **13**. The solvent was removed in vacuo and the crude product was purified by semi preparative HPLC to give **13** (2 mg, 22%) as an orange powder. HPLC: R_t: 23.2 min; IR (KBr): $\tilde{\nu}$=2201 (w), 2023 (m), 1904 (m), 1684 (m), 1601 cm^{-1} (s); ESI-MS: m/z: 1578.76 $[M+H]^+$, 1550.61 $[M-CO]^+$, 788.84 $[M]^{2+}$.

CCDC-632603 and CCDC-632604 contain the supplementary data for this paper. These data can be obtained free of charge from The Cambridge Crystallographic Data Centre via www.ccdc.cam.ac.uk/data_request/cif.

Acknowledgement

This work was supported by Mallinckrodt Med. Inc. Petten NL. We thank Dr. H. Schmalle for support in one of the X-ray structure analyses.

[1] S. Liu, *Chem. Soc. Rev.* **2004**, *33*, 445–461.
[2] S. M. Okarvi, *Med. Res. Rev.* **2004**, *24*, 685–686.
[3] P. Blower, *Dalton Trans.* **2006**, 1705–1711.
[4] C. von Sonntag, M. Dizdaroglu, *Carbohydr. Res.* **1977**, *58*, 21–30.
[5] B. Halliwell, J. M. C. Gutteridge, *Free Radical Res.* **1998**, *29*, 469–486.
[6] C. R. Silva, J. O. Valsa, M. S. Canine, A. Caldeira-de-Araujo, M. Bernardo-Filho, *Yale J. Biol. Med.* **1998**, *71*, 7–14.
[7] K. E. Bullok, S. T. Gammon, S. Violini, A. M. Prantner, V. M. Villalobos, V. Sharma, D. Piwnica-Worms, *Mol. Imaging* **2006**, *5*, 1–15.
[8] J. Yu, D. Parker, R. Pal, R. A. Poole, M. J. Cann, *J. Am. Chem. Soc.* **2006**, *128*, 2294–2299.
[9] A. R. Cowley, J. Davis, J. R. Dilworth, P. S. Donnelly, R. Dobson, A. Nightingale, J. M. Peach, B. Shore, D. Kerr, L. Seymour, *Chem. Commun.* **2005**, 845–847.
[10] P. Häfliger, N. Agorastos, B. Spingler, O. Georgiev, G. Viola, R. Alberto, *ChemBioChem* **2005**, *6*, 414–421.
[11] K. E. Bullok, M. Dyszlewski, J. L. Prior, C. M. Pica, V. Sharma, D. Piwnica-Worms, *Bioconjugate Chem.* **2002**, *13*, 1226–1237.
[12] T. M. Behr, G. Sgouros, V. Vougioukas, S. Memtsoudis, S. Gratz, H. Schmidberger, R. D. Blumenthal, D. M. Goldenberg, W. Becker, *Int. J. Cancer* **1998**, *76*, 738–748.
[13] G. L. Griffiths, S. V. Govindan, G. Sgouros, G. L. Ong, D. M. Goldenberg, M. J. Mattes, *Int. J. Cancer* **1999**, *81*, 985–992.
[14] T. M. Behr, M. Behe, M. Lohr, G. Sgouros, C. Angerstein, E. Wehrmann, K. Nebendahl, W. Becker, *Eur. J. Nucl. Med.* **2000**, *27*, 753–765.
[15] S. R. Nagalla, B. J. Barry, A. M. Falick, B. W. Gibson, J. E. Taylor, J. Z. Dong, E. R. Spindel, *J. Biol. Chem.* **1996**, *271*, 7731–7737.
[16] S. Mundwiler, M. Kündig, K. Ortner, R. Alberto, *Dalton Trans.* **2004**, 1320–1328.
[17] P. Häfliger, N. Agorastos, A. Renard, G. Giambonini-Brugnoli, C. Marty, R. Alberto, *Bioconjugate Chem.* **2005**, *16*, 582–587.
[18] B. E. Bowler, K. J. Ahmed, W. I. Sundquist, L. S. Hollis, E. E. Whang, S. J. Lippard, *J. Am. Chem. Soc.* **1989**, *111*, 1299–1306.
[19] H. J. Pietzsch, A. Gupta, R. Syhre, P. Leibnitz, H. Spies, *Bioconjugate Chem.* **2001**, *12*, 538–544.
[20] C. A. Hunter, J. K. M. Sanders, *J. Am. Chem. Soc.* **1990**, *112*, 5525–5534.
[21] C. J. Smith, G. L. Sieckman, N. K. Owen, D. L. Hayes, D. G. Mazuru, R. Kannan, W. A. Volkert, T. J. Hoffman, *Cancer Res.* **2003**, *63*, 4082–4088.
[22] M. B. Lyles, I. L. Cameron, *Biophys. Chem.* **2002**, *96*, 53–76.
[23] J. K. Frost, H. W. Tyrer, N. J. Pressman, C. D. Albright, M. H. Vansickel, G. W. Gill, *J. Histochem. Cytochem.* **1979**, *27*, 545–551.
[24] J. F. Golden, S. S. West, *J. Histochem. Cytochem.* **1974**, *22*, 495–505.
[25] V. Wing-Wah Yam, K.-W. L. , C. Kung-Kai, R. Yuen-Chong Kong, *J. Chem. Soc. Dalton Trans.* **1997**, 2067–2072.
[26] F. Pierard, A. Del Guerzo, A. Kirsch-De Mesmaeker, M. Demeunynck, J. Lhomme, *Phys. Chem. Chem. Phys.* **2001**, *3*, 2911–2920.
[27] B. Norden, M. Kubista, T. Kurucsev, *Q. Rev. Biophys.* **1992**, *25*, 51–170.
[28] R. La Bella, E. Garcia-Garayoa, M. Bahler, P. Blauenstein, R. Schibli, P. Conrath, D. Tourwe, P. A. Schubiger, *Bioconjugate Chem.* **2002**, *13*, 599–604.
[29] R. Alberto, K. Ortner, N. Wheatley, R. Schibli, A. P. Schubiger, *J. Am. Chem. Soc.* **2001**, *123*, 3135–3136.
[30] R. Alberto, R. Schibli, A. Egli, A. P. Schubiger, *J. Am. Chem. Soc.* **1998**, *120*, 7987–7988.
[31] A. Wada, S. Kozawa, *J. Polym. Sci. Part A* **1964**, *2*, 853–864.
[32] G. J. Atwell, G. W. Rewcastle, B. C. Baguley, W. A. Denny, *J. Med. Chem.* **1987**, *30*, 664–669.

Received: January 9, 2007
Published online: March 23, 2007

